Check for updates

Fabrication and mechanical properties of knitted dissimilar polymeric materials with movable cross-links†

Ryohei Ikura, [iD] [a] Shunsuke Murayama,[b] Junsu Park, [iD] [a] Yuka Ikemoto, [iD] [c] Motofumi Osaki, [iD] [d] Hiroyasu Yamaguchi, [iD] [aef] Akira Harada, [iD] [g] Go Matsuba [iD] *[b] and Yoshinori Takashima [iD] *[adef]

Bulk polymerization of liquid main chain monomers in the presence of a linear polymer bearing acetylated γ-cyclodextrin (TAcγCD) (primary polymer) results in composite materials consisting of dissimilar polymer chains, hereinafter called the designs of movable cross-network elastomer knitting dissimilar polymers (KP elastomers). The post polymerized chains (secondary polymer) penetrate cavities in the TAcγCD units and form movable cross-links that connect between the primary and secondary polymers. The KP elastomers successfully improve the mechanical properties based on two key design components. One is a long movable range. The secondary polymers easily move in the TAcγCD cavities on the primary polymers due to the lack of a chemical cross-linker between the primary and secondary polymers. Thus, the KP elastomers exhibit high toughness because the movable cross-links are not fixed, which results in effective stress dispersion. The other is the synergistic effect of the multiphase structure. The network designs of the KP elastomers enable composite materials with movable cross-links that can even connect immiscible polymers, namely, poly(ethyl acrylate) (PEA) and polystyrene (PS). The obtained materials contain a three-phase structure: PEA, PS, and a mixed phase. The synergistic effect of the three-phase structure simultaneously improves the toughness and stiffness.

Design, System, Application

Movable cross-linked materials connecting between dissimilar polymers were designed by the methods for the formation of movable cross-links "polymer threading through polymerization". We carried out the bulk polymerization of liquid main chain monomers in the presence of a linear polymer bearing TAcγCD units. The network designs of the obtained elastomers (KP elastomer) successfully improve the mechanical properties based on two key-systems. One is a long movable range. The KP elastomers exhibit high toughness because the movable cross-links are not interlocked, which results in effective stress dispersion. The other is the synergistic effect of the multiphase structure: PEA (contributing effective stress dispersion with high mobility), PS (contributing high stiffness and strength as hard domain), and a mixed phase (connecting each phase to work together). Blending of immiscible polymers cannot improve mechanical properties due to severe phase separation. However dissimilar knitting methods successfully improve toughness and stiffness of polymeric materials by the synergistic effect of the three-phase structure. These designs allow the application for extension of lifetime of products that can also promote the replacement of heavy materials (metals and ceramics) with lightweight polymeric materials.

Introduction

With increasing interest in establishing a sustainable society, the demand for tougher polymeric materials is increasing daily. Polymers with improved toughness can reduce waste by extending the lifetime of products. This can also promote the replacement of heavy materials (metals and ceramics) with lightweight polymeric materials, leading to a reduction in

[a] *Department of Macromolecular Science, Graduate School of Science, Osaka University, Toyonaka, Osaka 560-0043, Japan.*
E-mail: takasima@chem.sci.osaka-u.ac.jp
[b] *Graduate School of Organic Material Engineering, Yamagata University, 4-3-16 Jonan, Yonezawa, Yamagata 992-8510, Japan.*
E-mail: gmatsuba @yz.yamagata-u.ac.jp
[c] *Japan Synchrotron Radiation Research Institute, Sayo-gun, Hyogo 679-5198, Japan*
[d] *Institute for Advanced Co-Creation Studies, Osaka University, Toyonaka, Osaka 560-0043, Japan*

[e] *Project Research Center for Fundamental Sciences, Graduate School of Science, Osaka University, Machikaneyama-cho, Toyonaka, Osaka 560-0043, Japan*
[f] *Innovative Catalysis Science Division, Institute for Open and Transdisciplinary Research Initiatives (ICS-OTRI), Osaka University, Suita, Osaka 565-0871, Japan*
[g] *SANKEN (The Institute of Scientific and Industrial Research), Osaka University, IbarakiOsaka 567-0047, Japan*
† Electronic supplementary information (ESI) available: Preparative methods, NMR and FT-IR spectra, GPC, TGA, DMA, and SAXS measurements, mechanical properties and structures. See DOI: 10.1039/d2me00016d

fuel consumption. In recent decades, many efforts, such as the addition of filler,[1–4] polymer blending[5–7] and minimization of structural defects[8,9] have been attempted to prepare tougher polymeric materials.

Regarding polymers with enhanced toughness, three broad categories of polymer networks have been designed based on their stress dispersion properties. One is interpenetrating brittle and ductile networks.[10–14] The brittle network acts as sacrificial bonds, which dissipate stress and prevent catastrophic crack propagation. Another is a reversible cross-linked network. The reversible cross-links are constructed by dynamic covalent bonds[15–17] and noncovalent bonds.[18–52] These bonds are usually weaker than covalent bonds and act as sacrificial bonds. The other type is a movable cross-linked network that disperses stress based on the mobility of cross-links along the axis of the polymers.[53,54]

The preparation methods for movable cross-linked materials fall into five broad categories. These methods are based on macrocyclic molecules, and these ring-shaped molecules enable us to construct supramolecular architectures, such as pseudo-rotaxane/rotaxane,[55] pseudo-polyrotaxane/polyrotaxane,[56–58] catenane/polycatenane,[59,60] and [c2]-daisy chains.[61–64] The first method is "connecting between the ring units of polyrotaxane".[54,65–73] The second method is "polymerization of the polymerizable groups on the ring units of polyrotaxane".[74–79] Reversible cross-linked materials prepared from polyrotaxane were also studied.[80–86] The third method is "formation of a rotaxane/polyrotaxane structure in a side chain".[87–95] The fourth method is "the polycondensation of the inclusion complex".[96–110]

Previously, we prepared elastomers with movable cross-links by copolymerization between CD monomers and main chain monomers (single movable cross-network (SC) elastomers)[111,112] (Fig. 1), which is the fifth method "polymer threading through polymerization".[111–114] SC elastomers show a higher toughness and Young's modulus than covalently cross-linked elastomers.[112] Inoue and his coworker revealed that improvements in the mechanical properties of SC elastomers were derived from the viscoelastic behavior and relaxation mode of the movable cross-links.[115,116] Notably, the advantage of the fifth method is an easy preparation of movable cross-linked materials through the polymerization of vinyl monomers. By expanding the fifth method, the combination of two dissimilar polymers using movable cross-links will improve the toughness and Young's modulus of the material.

Herein, we aimed to improve the mechanical properties by two design strategies: (I) a longer movable range for effective stress dispersion and (II) a combination of hard primary polymers with a high Young's modulus and soft secondary polymers for effective stress dispersion (Fig. 1). To realize these design strategies, we invented an elastomer with movable cross-links that connect dissimilar polymers in two steps. First, we copolymerized the peracetylated γCD (TAcγCD) monomer and main chain monomer in organic solution to obtain the host polymer (primary polymer). Next, we polymerized another liquid main chain monomer in the
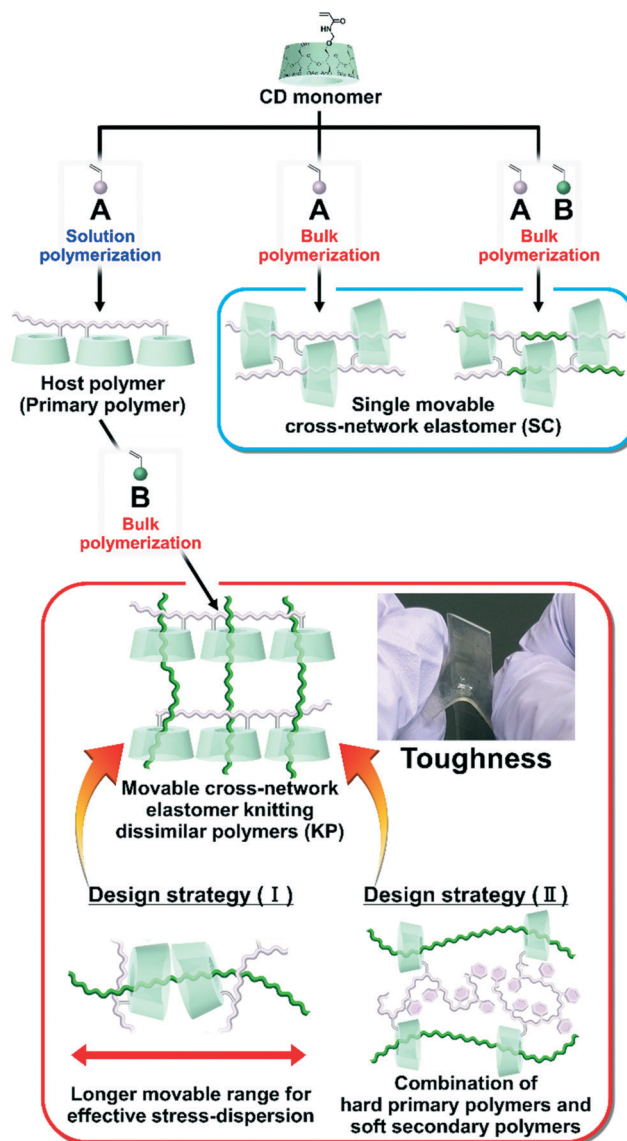

Fig. 1 Routes toward two different material designs with movable cross-links: single movable cross–network elastomer (SC)[115,116] and movable cross–network elastomer for knitting dissimilar polymers (KP). KP elastomers allow for the two design strategies: (I) and (II).

presence of a host polymer. The post polymerized chains (secondary polymer) penetrate the TAcγCD units and form movable cross-links that connect the dissimilar polymers. This knitting of primary and secondary polymers results in an elastomer (KP elastomer) that consists of host monomer-penetrated movable cross-links and dissimilar polymers. This report focuses on the mechanical properties of the KP elastomers with regard to the network designs, stress dispersion behavior, and domain structures.
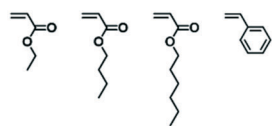
Results and discussion

2-1. Preparation of the KP elastomers

Fig. 2 shows the chemical structures of the main chain monomers, primary polymers, KP elastomers, SC elastomers,
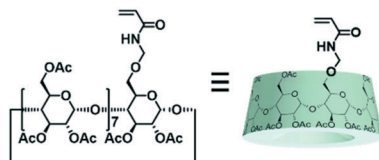
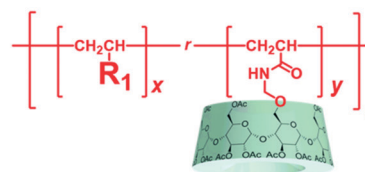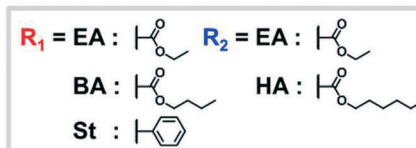**Fig. 2** Chemical structures of (a) the main chain monomers (EA, BA, HA, and St), the peracetylated CD monomer (TAcγCDAAmMe), (b) the primary polymers (PR$_1$–PAcγCD (x, y)), (c) the KP elastomers (PR$_1$–CD (x, y)⊃PR$_2$ (z)), the SC elastomers (P(R$_1$–R$_2$)–CD (x, y, z)), and the polymer blends (PR$_1$(x)/PR$_2$(y)).
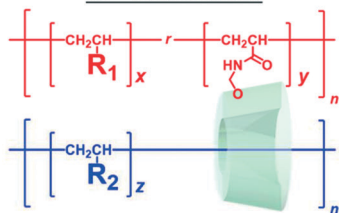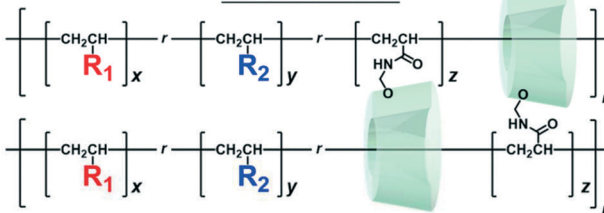
and polymer blends. Ethyl acrylate (EA), butyl acrylate (BA), hexyl acrylate (HA), and styrene (St) were employed as the liquid main chain monomers (Fig. 2a). To solubilize in hydrophobic solvent, peracetylated CD monomer (mono-6O-acrylamidomethyl-triicosaacetyl-γ-cyclodextrin; abbreviated TAcγCDAAmMe) was prepared according to a previous report.[43]

The primary polymers were obtained by solution copolymerization between main chain monomer R$_1$ and TAcγCD monomer in hydrophobic solvents (chloroform or toluene) (Schemes S1–S3 and Tables S1–S3†). The solvents act as competitive guests to prevent the formation of movable cross-links in the primary polymers.[111] The obtained primary polymers are abbreviated PR$_1$–CD PP (x, y), where x and y are the mol% contents of the R$_1$ and TAcγCD units, respectively. PR$_1$ (poly(R$_1$); a homopolymer without TAcγCD units) was also prepared by solution polymerization (Schemes S4 and S5†).

The KP elastomers were obtained by the bulk polymerization of another main chain monomer R$_2$ in the presence of PR$_1$–CD PP (x, y) (Schemes S6–S8 and Tables S4–S6†). The obtained KP elastomers were abbreviated PR$_1$–CD (x, y)⊃PR$_2$ (z), where x, y, and z are the mol% contents of the R$_1$, TAcγCD, and R$_2$ units, respectively. The TAcγCD units form movable cross-links between the PEA chains.[111] Therefore, EA was mainly employed as the main chain monomer for the secondary polymer. As control samples to investigate the properties derived from network structures,

P(R$_1$–R$_2$)–CD (x, y, z) (SC elastomers) were obtained from bulk polymerization (Scheme S9 and Table S7†). PR$_1$(x)/PR$_2$(y) (polymer blends) were obtained from bulk polymerization in the presence of the homopolymer (Schemes S10 and S11†). PEA–CD (x, y) and PEA were prepared according to a previous report[111] Almost quantitively polymerization reactions were confirmed from integral values of [1]H-nuclear magnetic resonance (NMR) spectra and absence of C═C peaks in the ^{13}C-NMR and Fourier transform infrared (FT-IR) spectra (Fig. S3–35†).

2-2. Mechanical properties of the KP elastomers

The mechanical properties of the KP elastomers were investigated by tensile tests (Fig. 3, S37, S38, and Table S10†). Prior to the KP elastomers with dissimilar polymers, tensile tests of PEA–CD (20, 1)⊃PEA (79) and control elastomers (PEA–CD (99, 1) and PEA) were carried out to reveal the effect of the structure itself. As a results, PEA–CD (20, 1)⊃PEA (79) showed the highest fracture stress and strain. Toughness was calculated from the integral of the stress–strain curve representing the tensile test results. Fig. 3a shows plots of the relation between the toughness and Young's moduli of PEA–CD (20, 1)⊃PEA (79). The toughness and Young's modulus of PEA–CD (20, 1)⊃PEA (79) were 16 ± 1 and 5.5 ± 2.2 times higher than those of PEA, indicating the presence of TAcγCD units as cross-linkers. Interestingly, the toughness
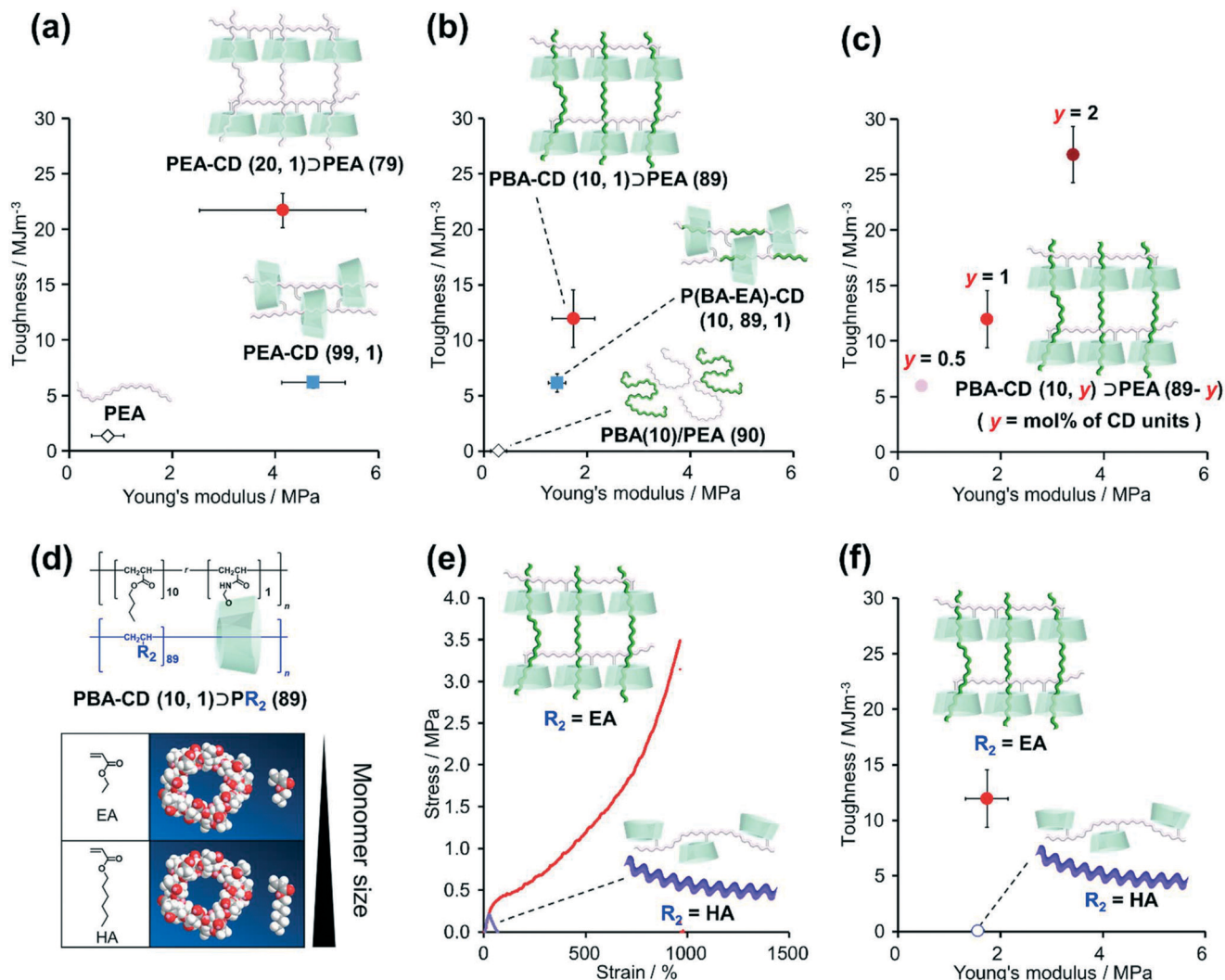
Fig. 3 Plots of the toughness and Young's modulus of (a) PEA–CD (20, 1)⊃PEA (79) (red filled circle), PEA–CD (99, 1) (blue filled square), PEA (black open rhombus), (b) PBA–CD (10, 1)⊃PEA (89) (red filled circle), P(BA–EA)–CD (10, 89, 1) (blue filled square), PBA(10)/PEA(90) (black open rhombus), (c) PBA–CD (10, y)⊃PEA (10-y) (y = 0.5: pale red filled circle, y = 1: red filled circle, and y = 2: dark red filled circle). (d) 3D models (Chem3D® Ultra 16.0.1.4) of TAcγCD, EA, and HA. (e) Stress–strain curves of PBA–CD (10, 1)⊃PEA (89) (red line) and PBA–CD (10, 1)⊃PHA (89) (purple line). (f) Plots of the toughness and Young's modulus of PBA–CD (10, 1)⊃PEA (89) (red filled circle) and PBA–CD (10, 1)⊃PHA (89) (purple open circle).

of PEA–CD (20, 1)⊃PEA (79) was 3.5 ± 0.2 times higher than that of PEA–CD (99, 1), indicating that the network structure of PEA–CD (20, 1)⊃PEA (79) resulted in a higher toughness.

Similar results were obtained with the KP elastomers with dissimilar polymers and their control samples. PBA–CD (10, 1)⊃PEA (79) also showed the highest strength and stretchability (Fig. S37 and Table S10†). PBA–CD (10, 1)⊃PEA (79) exhibited clear fracture points and (6.4 ± 1.4) × 10^2 times and 6.2 ± 1.5 times higher toughness and Young's moduli compared with PBA(10)/PEA (90), confirming the formation of movable cross-links (Fig. 3b). PBA–CD (10, 1)⊃PEA (89) showed a 1.9 ± 0.4 times higher toughness than P(BA–EA)–CD (10, 89, 1). Fig. 3c shows the relation between the toughness and Young's modulus of PBA–CD (10, y)⊃PEA (10-y) (mol% of TAcγCD units: y = 0.5, 1, and 2). With increasing TAcγCD units, the toughness

and Young's moduli of PBA–CD (10, y)⊃PEA (10-y) increased. These results confirmed that the TAcγCD units acted as cross-links.

2-3. Relation between cross-link formation and secondary polymer diameter

We investigated the relation between the mechanical properties of the materials and the size of the secondary monomers EA and HA (Scheme S12†). Fig. 3d shows the 3D models (Chem3D® Ultra 16.0.1.4) of TAcγCD, EA, and HA. The structures of the models were generated by minimizing the internal energy of each molecule by MM2 molecular dynamics. As HA is larger than the cavity diameter of TAcγCD, we assumed that the poly(hexyl acrylate) (PHA) chains rarely penetrated TAcγCD.

736 | Mol. Syst. Des. Eng., 2022, 7, 733–745

This journal is © The Royal Society of Chemistry and IChemE 2022

Fig. 3e shows the stress–strain curves of PBA–CD (10, 1)⊃PEA (89) and PBA–CD (10, 1)⊃PHA (89). While PBA–CD (10, 1)⊃PEA (89) exhibited a clear fracture point, PBA–CD (10, 1)⊃PHA (89) showed plastic deformation. The toughness of PBA–CD (10, 1)⊃PHA (89) decreased to only 0.42% of that of PBA–CD (10, 1)⊃pEA (89) (Fig. 3f) despite having similar
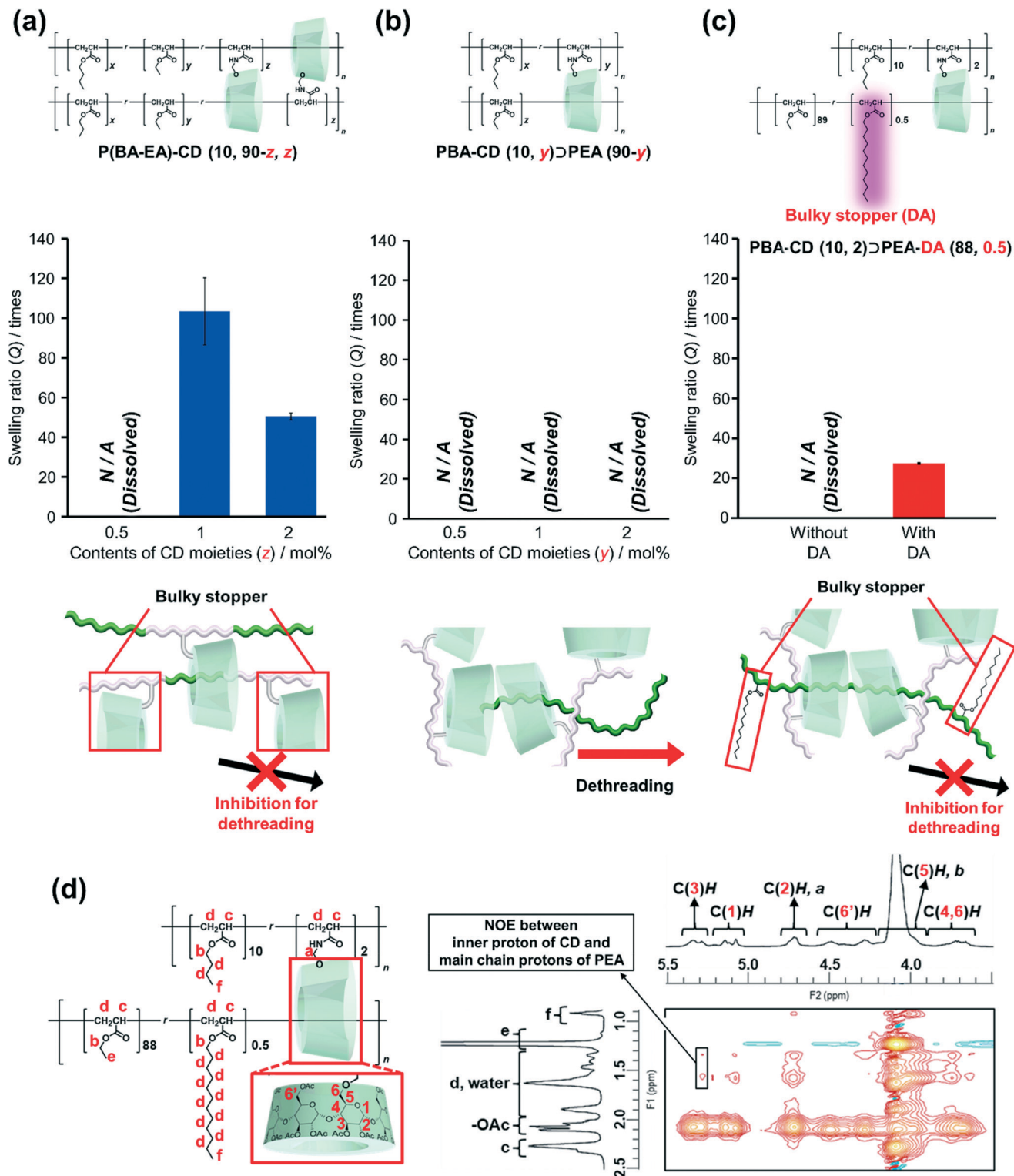
Fig. 4 Swelling ratios and proposed structures of (a) P(BA–EA)–CD (10, 90-z, z), (b) PBA–CD (10, y)⊃PEA (90-y), (c) PBA–CD (10, 2)⊃PEA-DA (88) and PBA–CD (10, 2)⊃PEA-DA (88, 0.5). Contents of the CD moieties were 0.5, 1, and 2. (d) 600 MHz 2D ^{1}H–^{1}H NOESY NMR spectrum of the PBA–CD (10, 2)⊃PEA-DA (88, 0.5) slurries with chloroform-d.

This journal is © The Royal Society of Chemistry and IChemE 2022

Mol. Syst. Des. Eng., 2022, **7**, 733–745 | **737**

Young's moduli. This implied that temporary cross-links formed between the TAcγCD units and chain ends or side chains of PHA instead of stable movable cross-links. These results supported our assumption from the 3D models, which suggested that the high toughness was due to complexation between the TAcγCD units and secondary polymers. SC elastomers with PBA linear polymer (PBA(10)/PEA–CD(89, 1)) show lower toughness than PBA–CD (10, 1)⊃PEA (89), supporting connection between dissimilar polymers improved mechanical properties (Scheme S13 and Fig. S39†).

2-4. Investigation of the network structure by swelling tests

To characterize the network structures, we conducted swelling tests using chloroform as the swelling solvent. The polymers were immersed in excess chloroform. The swelling ratio (Q) was determined by the following equation:

$$\text{Swelling ratio } (Q) = \frac{W - W_0}{W_0} \times 100\%$$

where W is the weight of the swollen polymer and W_0 is the initial weight of the polymer before swelling. The Q of the P(BA–EA)–CD (10, 90-z, z) (z = 0.5, 1, and 2) polymers decreased with increasing mol% content of the TAcγCD unit, indicating the formation of interlocked cross-links (Fig. 4a). On the other hand, all PBA–CD (10, y)⊃PEA (90-y) (y = 0.5, 1, and 2) samples dissolved in chloroform (Fig. 4b). These solubilities allowed the GPC measurements of the KP elastomers (Fig. S36, Tables S8, and S9†). The GPC profiles of KP elastomers showed two peaks with the order of molecular weights comparable to (i) primary polymers and (ii) PEA obtained by bulk polymerization, respectively. These results suggest that the dethreading of the secondary polymer from the TAcγCD units caused the elastomers to dissolve.

To confirm this presumption, we also prepared PBA–CD (10, 2)⊃PEA–DA (88, 0.5), where the secondary polymer contained bulky DA units to prevent the TAcγCD units from passing over (Scheme S14†). While PBA–CD (10, 2)⊃PEA (88) was dissolved, PBA–CD (10, 2)⊃PEA–DA (88, 0.5) was swollen to give a smaller Q than that of P(BA–EA)–CD (10, 88, 2) (Fig. 4c). These results indicated the presence of movable cross-links in PBA–CD (x, y)⊃PEA (z) between the TAcγCD units and secondary polymers.

2D nuclear Overhauser effect spectroscopy (NOESY) NMR spectra were obtained to confirm the complexation between the TAcγCD units and PEA. To prevent peak broadening, chloroform-d organogels of PBA–CD (10, 2)⊃PEA–DA (88, 0.5) were ball-milled into slurries before taking measurements. The spectrum of the ball-milled PBA–CD (10, 2)⊃PEA–DA (88, 0.5) slurries with chloroform-d exhibited NOE correlation signals between the protons in the TAcγCD units and PEA chains (Fig. 4d). Since C(3)H protons were located on the internal side of the TAcγCD rings, NOE signals of C(3)H indicated that the PEA main chains penetrated the TAcγCD units. On the other hand, the NOE signals of C(3)H were not observed in the spectrum of the reference sample: chloroform-d solutions of P(EA–DA) and PBA–CD PP(20, 1) (Fig. S40†). These results indicated that the TAcγCD units formed inclusion complexes with the PEA secondary polymer chains.

2-5. Investigation of the structural information by SAXS and DSC

To elucidate the deformation mechanism, we investigated nanoscale structures by small-angle X-ray scattering (SAXS) measurements upon tensile deformation. Fig. 5 shows the SAXS profiles of PBA(10)/PEA(90), P(BA–EA)–CD (10, 89, 1), and PBA–CD (10, 1)⊃PEA (89) with various λ strains (λ = 0%, 30%, 60%, 90%, and 120%) in the tensile and vertical directions. The intensities of the small scattering vector were in the order PBA(10)/PEA(90) > PBA–CD (10, 1)⊃PEA (89) > P(BA–EA)–CD (10, 89, 1) at λ = 0%. These results indicated that PBA–CD (10, 1)⊃PEA (89) was more homogenous than PBA(10)/PEA(90) but less homogeneous than P(BA–EA)–CD (10, 89, 1).

The intensities of PBA(10)/PEA(90) in the tensile direction decreased through deformation, indicating the orientation of the polymer chains. The streak-like scattering patterns of PBA(10)/PEA(90) supported the polymer orientation. Notably, P(BA–EA)–CD (10, 89, 1) did not show the orientation. The intensities of PBA–CD (10, 1)⊃PEA (89) in both directions increased through deformation, showing strain-induced phase separation between the primary and secondary polymers. The small orientation of PBA–CD (10, 1)⊃PEA (89) was also observed from the higher intensity in the vertical direction at a high value of λ. These results exhibited dethreading of the secondary polymer through deformation of the KP elastomers.

The thermal properties were also evaluated by differential scanning calorimetry (DSC) (Fig. S41†). PBA(10)/PEA(90) showed a characteristic endothermic peak after the endothermic transition step of glass transition temperature (T_g = −18 °C) of the PEA polymer. These peaks indicated that the PEA chains underwent enthalpy relaxation below T_g within the time scale of the cooling process in the measurements. Enthalpy relaxation is the structural relaxation of glass from nonequilibrium conformations toward an overall equilibrium state below T_g.[117,118] It is known that an increased number of cross-links restricts enthalpy relaxation.[119] The absence of the enthalpy relaxation peaks of PBA–CD (10, 1)⊃PEA (89) supported the formation of movable cross-links on the PEA secondary polymer. PEA–CD (20, 1)⊃PEA (79) and the reference samples also showed similar tendencies in their DSC results (Fig. S42†). In the thermal gravimetric analysis (TGA) results, PBA(10)/PEA(90) showed two steps of pyrolysis (below and above 360 °C). However, PBA–CD (10, 1)⊃PEA (89) showed one step of pyrolysis and higher thermostability at 350 °C than PBA(10)/PEA(90) (Fig. S43†). Those results could be contributed by the improvement of homogeneity by the formation of movable
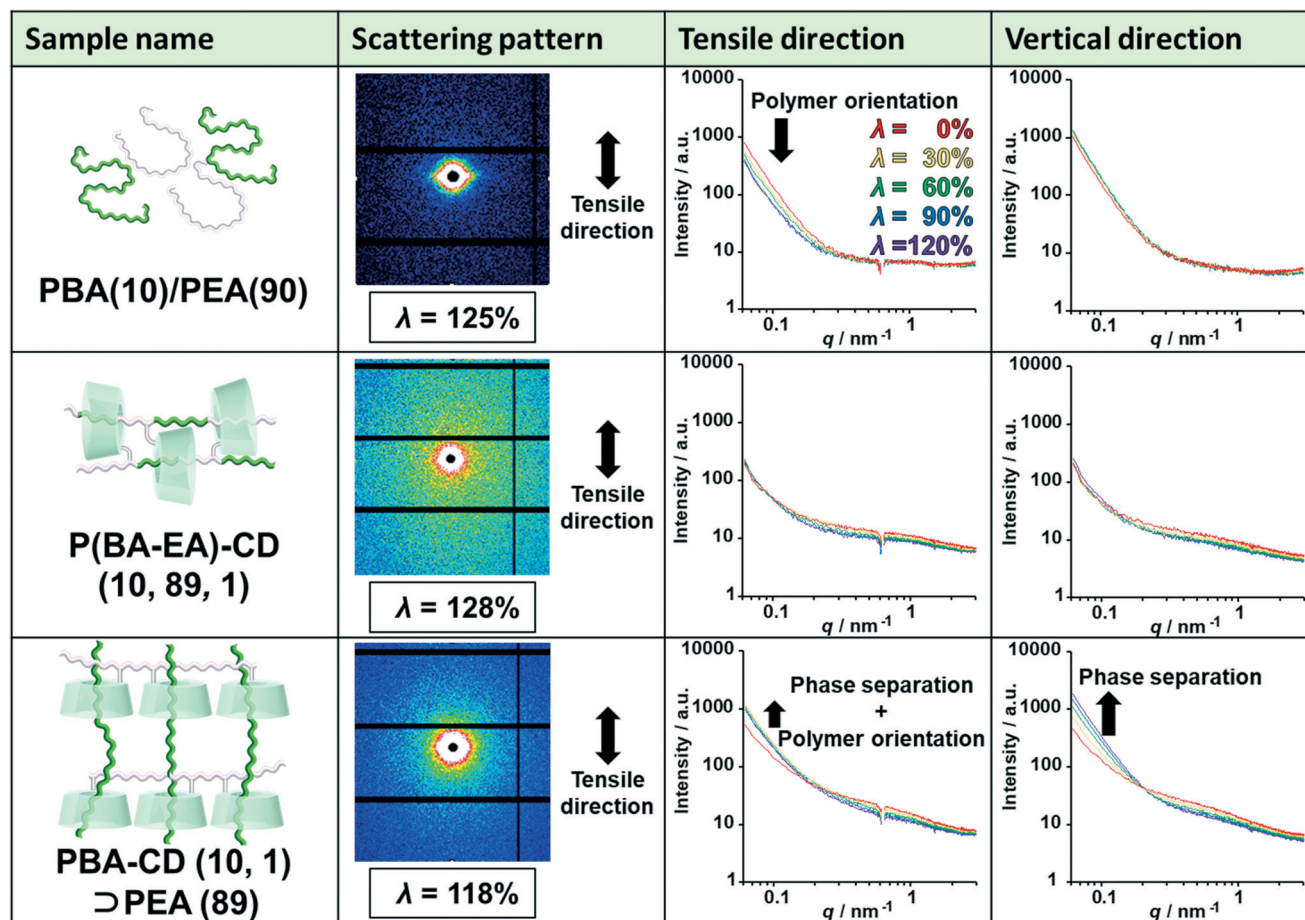
738 | *Mol. Syst. Des. Eng.*, 2022, **7**, 733–745

This journal is © The Royal Society of Chemistry and IChemE 2022

Fig. 5 Scattering patterns of PBA(10)/PEA(90) with 125% strain, P(BA–EA)–CD (10, 89, 1) with 128% strain, and PBA–CD (10, 1)⊃PEA (89) with 118% strain. SAXS profiles of PBA(10)/PEA(90), P(BA–EA)–CD (10, 89, 1), and PBA–CD (10, 1)⊃PEA (89) with λ strains (λ = 0%: red line, λ = 30%: yellow line, λ = 60%: green line, λ = 90%: blue line, and λ = 120%: purple line) in the tensile and vertical directions.

cross-links between primary and secondary polymers. Furthermore, compared to PEA, PEA–CD (20, 1)⊃PEA (79) also showed higher thermostability at 350 °C (Fig. S44†).

2-6. Evaluation of the stress dispersion property by stress-relaxation tests

To clarify relationship between the time scale of deformation and stress dispersion against strain, we performed tensile tests of two kinds of movable cross-linked materials with various tensile rates $\dot{\lambda}$ ($\dot{\lambda}$ = 1.0, 0.30, 0.10, 0.030, and 0.010 mm s^{-1}). While the stress of P(BA–EA)–CD (10, 89, 1) decreased with decreasing tensile rate, the fracture strain values are not significantly changed by the tensile rate (Fig. 6a). PBA–CD (10, 1)⊃PEA (89) exhibited elastic behavior at $\dot{\lambda}$ = 1.0 and 0.30 mm s^{-1} (Fig. 6b). The tensile strain drastically improved at $\dot{\lambda}$ = 0.10 and 0.030 based on the effective mobility of the cross-links and dethreading. At too slow of a tensile rate ($\dot{\lambda}$ = 0.010), the movable cross-links in PBA–CD (10, 1)⊃PEA (89) lost elasticity to result in plastic deformation like polymeric materials without solid cross-link. While the slow deformation is supposed to be derived from effective mobility of the movable

cross-links, the interlocked cross-links of P(BA–EA)–CD (10, 89, 1) prevent improved fracture strain. Dethreading of secondary polymers in PBA–CD (10, 1)⊃PEA (89) were also observed in cyclic tensile tests (Fig. S45†).

Mentioned in Introduction, the high mechanical properties of the movable cross-linked materials were attributed to the stress dispersion properties at the cross-linking points. Herein, we carried out stress-relaxation tests to compare the stress dispersion properties between two kinds of movable cross-linked materials. The test pieces were continuously stretched until reaching 400%. Then, the test piece was held at the strain 400%, and the stress of the test piece was recorded for 3000 s (Fig. 6c). At the start of the stress-relaxation tests, the stress of PBA–CD (10, 1)⊃PEA (89) was higher than that of P(BA–EA)–CD (10, 89, 1). However, the stress of the former became lower than the latter in approximately 60 s. Consequently, PBA–CD (10, 1)⊃PEA (89) showed a smaller residual stress than P(BA–EA)–CD (10, 89, 1). These results suggested that PBA–CD (10, 1)⊃PEA (89) dispersed the internal stress more effectively.

To obtain further insight into the stress-relaxation behavior of these movable cross-linked materials, we carried
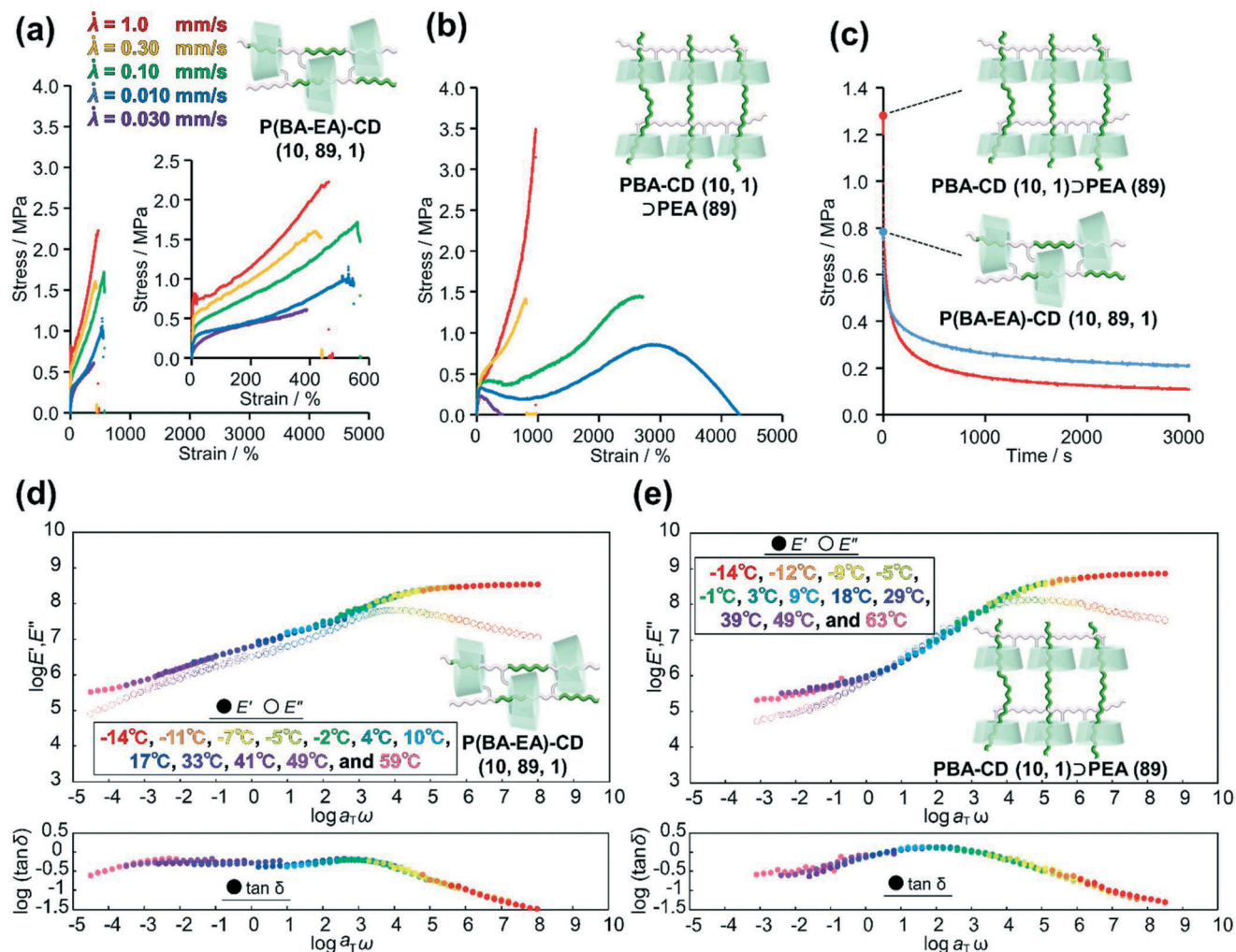
This journal is © The Royal Society of Chemistry and IChemE 2022

Mol. Syst. Des. Eng., 2022, **7**, 733–745 | **739**

Fig. 6 Stress strain curves of (a) PBA–CD (10, 1)⊃PEA (89) and (b) P(BA–EA)–CD (10, 89, 1) with a $\dot{\lambda}$ tensile rate ($\dot{\lambda}$ = 1.0 mm s⁻¹: red line, $\dot{\lambda}$ = 0.30 mm s⁻¹: yellow line, $\dot{\lambda}$ = 0.10 mm s⁻¹: green line, $\dot{\lambda}$ = 0.030 mm s⁻¹: blue line, and $\dot{\lambda}$ = 0.0010 mm s⁻¹: purple line). (c) Stress relaxation of PBA–CD (10, 1)⊃PEA (89) and P(BA–EA)–CD (10, 89, 1) at 400% strain. Composite curves of the logarithmic moduli (log E' and log E'') and log(tan δ) of (d) P(BA–EA)–CD (10, 89, 1) and (e) PBA–CD (10, 1)⊃PEA (89).

out curve fitting using the Kohlrausch–Williams–Watts models, as described by the following equation. Notably, the stress σ *versus* relaxation time t curves were well fitted ($R^2 > 0.99$) (Fig. S46†).

$$\sigma = \sigma_r \exp\left\{-\left(\frac{t}{\tau}\right)^{\beta}\right\} + \sigma_{\infty}$$

In the above equation, σ_r is the relaxable stress, σ_{∞} is the residual stress, τ is the time constant, and β is the stretching

exponent. The obtained fitting parameters are summerized in Table 1. Consequently, PBA–CD (10, 1)⊃PEA (89) showed faster and larger stress dispersion, leading to its high toughness shown in the tensile test.

Fig. 6d and e show the composite curves of the logarithmic storage and loss moduli (log E' and log E'') and log(tan δ) (tan δ = E''/E') of P(BA–EA)–CD (10, 89, 1) and PBA–CD (10, 1)⊃PEA (89) obtained from dynamic mechanical analysis (DMA; see ESI† for detail). The composite curves of the E' and E'' were constructed following the time (angular frequency)-temperature superposition principle: each

Table 1 Obtained fitting parameters using the KWW models

	Relaxable component			Residual components
	σ_r (MPa)	τ (s)	β	σ_{∞} (MPa)
P(BA–EA)–CD (10, 89, 1)	0.67	140	0.29	0.15
PBA–CD (10, 1)⊃PEA (89)	1.33	30	0.29	0.07

740 | *Mol. Syst. Des. Eng.*, 2022, **7**, 733–745

This journal is © The Royal Society of Chemistry and IChemE 2022

modulus was a horizontally shifted modulus using the horizontal shift factor, α_T, and a reference temperature (20 °C). Since the time–temperature superposition principle gave well-fitted composite curves, here we discuss the dynamics of polymer chain using the composite curves. Relaxations of E' and E'' for PBA–CD (10, 1)⊃PEA (89) were observed at higher frequency than those of P(BA–EA)–CD (10, 89, 1). In addition, PBA–CD (10, 1)⊃PEA (89) showed higher peaks of tan δ than P(BA–EA)–CD (10, 89, 1). These results showed a faster and larger relaxation mode of PBA–CD (10, 1)⊃PEA (89) at $\omega = 10^{-2}$–10^4 rad per s. In addition, PBA–CD (10, 1)⊃PEA (89) exhibited a lower activation energy than P(BA–EA)–CD (10, 89, 1) (Fig. S48†), suggesting lower energy barrier for the relaxation. These results supported the effective stress dispersion over a longer movable range to realize high toughness. PEA–CD (99, 1) and PEA–CD (10, 1)⊃PEA (89) also showed similar tendencies in their DMA results (Fig. S47 and S48†).

2-7. Preparation of the KP elastomers with immiscible polymers and their mechanical properties

As mentioned above, the homogeneity of PBA–CD (10, 1)⊃PEA (89) was improved by the movable cross-links that connected the primary and secondary polymers. Herein, PEA and PS were employed as primary and secondary polymers, respectively. The combination of these polymers was reported to have very low miscibility (<0.01 wt% of PEA in PS).[120]

The polymer blend without cross-links PS (20)/PEA (80) showed phase separation, forming heterogeneous domains on the order of 0.1 mm (Fig. 7a). The KP elastomers PS–CD (20, 1)⊃PEA (79) with immiscible polymers were white elastomers without heterogeneous domains on the order of 0.1 mm. These results confirmed an (i) improved miscibility and (ii) phase separation in the obtained elastomer. PS–CD (20, 1)⊃PEA (79) showed a 170 ± 30 times increase in

toughness and 1.6 ± 0.3 times increase in the Young's modulus of PS (20)/PEA (80), indicating the formation of movable cross-links between the primary and secondary polymers (Fig. 7b, S49, and Table S11†). Interestingly, PS–CD (20, 1)⊃PS (79) exhibited a 1.6 ± 0.3 times increase in toughness and a 8.2 ± 0.4 times increase in the Young's modulus of the KP elastomers with similar polymers PEA–CD (20, 1)⊃PEA (79).

To obtain further insight into the phase separation, we performed DSC measurements. PS–CD (20, 1)⊃PEA (79) showed three T_g steps at −12, 40 and 101 °C (Fig. S50†). The transition at −12 °C represented the T_g of the PEA secondary polymer in PS–CD (20, 1)⊃PEA (79). The high mobility of the secondary polymer resulted in effective stress dispersion by the movable cross-links. The SAXS measurements of PS–CD (20, 1)⊃PEA (79) showed the dethreading of the secondary polymer upon deformation, supporting the high mobility of the secondary polymers and movable cross-links (Fig. S51†). The transition at 101 °C represented the T_g of the PS primary polymer, which acted as a hard domain to give a high fracture stress and Young's modulus. The transition at 40 °C represented a compatible phase between PEA and PS in PS–CD (20, 1)⊃PEA (79). In contrast, heterogeneous PS (20)/PEA (80) did not show this step. In DMA measurements of PS–CD (20, 1)⊃PEA (79), E' and E'' at 60 °C drastically decreased beyond to fit composite curves (Fig. S52†). These results supported that the movable cross-links improved the compatibility of the polymers, enabling the multiphase structure to work collaboratively. The improved compatibility was also supported by the one pyrolysis step of PS–CD (20, 1)⊃PEA (79) in the TGA results (Fig. S53†). The higher compatibilities allows the improvements of thermal stabilities of PEA chains by chain transfer, in which terminal radicals of depolymerizing PEA chains were trapped by tertiary protons in PS chains.[121–123] Consequently, movable cross-links between immiscible
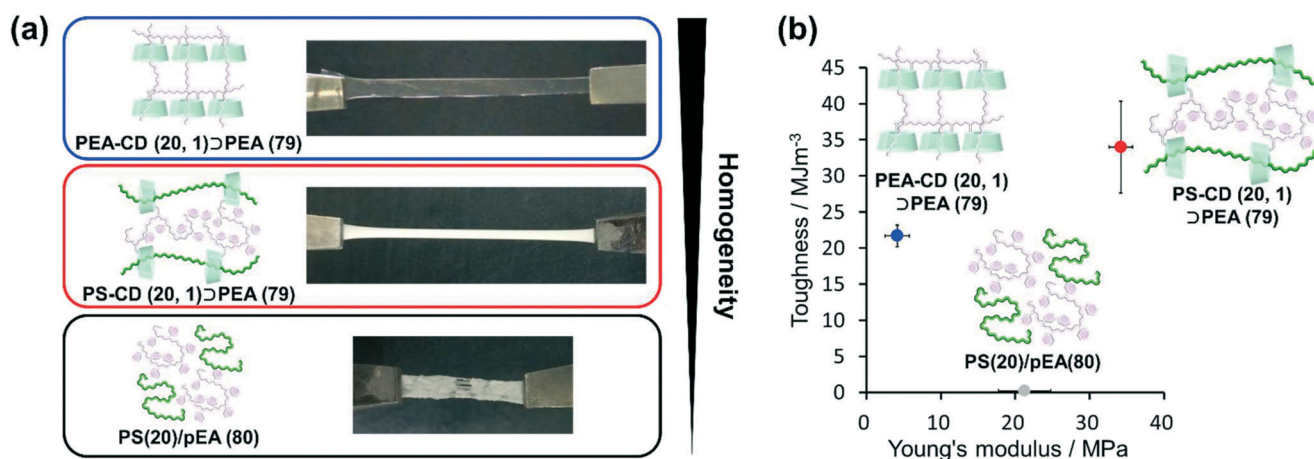

Fig. 7 (a) Photographs and (b) plots of the toughness and Young's modulus of PS–CD (20, 1)⊃PEA (79) (red filled circle), PEA–CD (20, 1)⊃PEA (79) (blue filled circle), and PS(20)/PEA(80) (black open rhombus). (c) DSC curves of PS–CD (20, 1)⊃PEA (79) (red line), PEA–CD (20, 1)⊃PEA (79) (blue line), and PS(20)/PEA(80) (gray line).

This journal is © The Royal Society of Chemistry and IChemE 2022

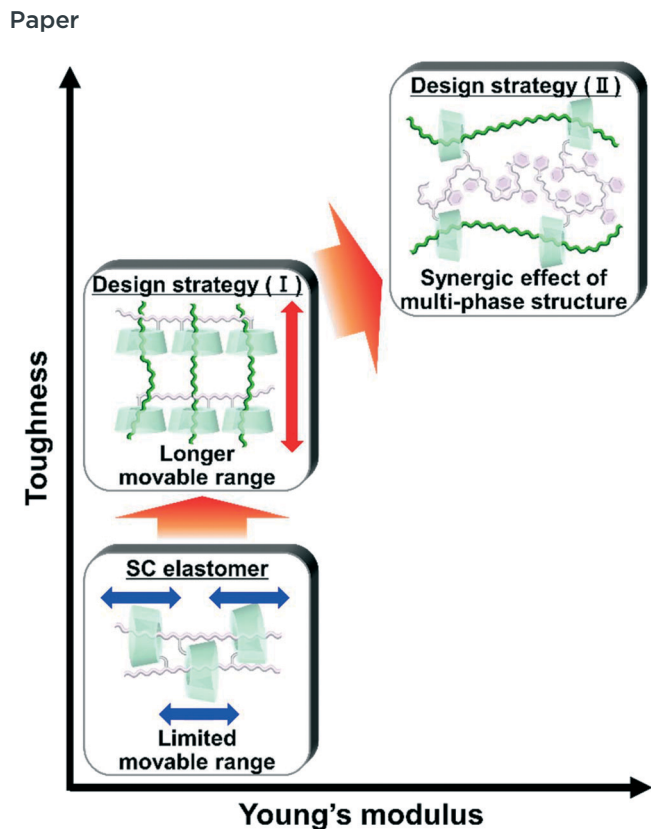*Mol. Syst. Des. Eng.*, 2022, **7**, 733–745 | 741

Fig. 8 Achieving a higher toughness and Young's modulus by the two design strategies.

polymers realized a three-phase structure to simultaneously achieve a high toughness and Young's modulus.

Conclusion

We conducted free-radical polymerization of a main chain monomer in the presence of a linear polymer with TAcγCD (primary polymer). The post polymerized chains (secondary polymer) penetrate the TAcγCD units and act as movable cross-links that connect the two dissimilar polymers. The obtained KP elastomers have a longer movable range than the one-pot fabricated materials with movable cross-links (Fig. 8). The secondary polymers have no bulky stopper, allowing dethreading upon tensile deformation. The larger movable range results in faster and more effective stress dispersion to achieve higher toughness. In addition, we successfully prepared even tougher and stiffer materials using movable cross-links to connect immiscible polymers (PEA and PS). These materials contain a three-phase structure: PEA, PS and a mixed phase. The PEA phase contributes to effective stress dispersion by the movable cross-links on account of its low T_g and high mobility. The PS phase contributes to a high fracture stress and Young's modulus as a hard domain with a high T_g (~100 °C). The movable cross-links connect the two phases and result in a mixed phase, enabling each phase to work together. These findings should provide design strategies for simultaneously enhancing the toughness, stiffness, and compatibility of polymeric materials and their composites.

Author contributions

Y. T. conceived and directed the study. R. I. performed syntheses and spectroscopic studies. All authors contributed to characterizations and discussion. Y. I. discussed and explained the results of the FT-IR spectroscopies. S. M. and G. M. discussed and explained the results of the SAXS measurements. M. O. wrote a section relating with DMA measurements. R. I., J. P., and Y. T. co-wrote the paper. A. H. and H. Y. gave valuable suggestions. Y. T. oversaw the project as well as contributed to the execution of the experiments and interpretation of the results.

Conflicts of interest

There are no conflicts to declare.

Acknowledgements

References

1 J. N. Coleman, U. Khan, W. J. Blau and Y. K. Gun'ko, *Carbon*, 2006, **44**, 1624–1652.
2 G. G. Tibbetts, M. L. Lake, K. L. Strong and B. P. Rice, *Compos. Sci. Technol.*, 2007, **67**, 1709–1718.
3 T. Ramanathan, A. A. Abdala, S. Stankovich, D. A. Dikin, M. Herrera-Alonso, R. D. Piner, D. H. Adamson, H. C. Schniepp, X. Chen, R. S. Ruoff, S. T. Nguyen, I. A. Aksay, R. K. Prud'Homme and L. C. Brinson, *Nat. Nanotechnol.*, 2008, **3**, 327–331.

This journal is © The Royal Society of Chemistry and IChemE 2022

4   M. Nogi, S. Iwamoto, A. N. Nakagaito and H. Yano, *Adv. Mater.*, 2009, **21**, 1595–1598.

5   S. Wu, *J. Appl. Polym. Sci.*, 1988, **35**, 549–561.

6   S. Wu, *Polym. Eng. Sci.*, 1990, **30**, 753–761.

7   T. H. Courtney, *Mechanical Behavior of Materials*, Waveland Press Inc., Illinois, 2016.

8   N. Sasaki, T. Matsunaga, M. Shibayama, S. Suzuki, Y. Yamamoto, R. Yoshida, C. Ito, T. Sakai and U. Chung, *Macromolecules*, 2008, **41**, 5379–5384.

9   S. Kondo, T. Hiroi, Y. S. Han, T. H. Kim, M. Shibayama, U. Il Chung and T. Sakai, *Adv. Mater.*, 2015, **27**, 7407–7411.

10 J. P. Gong, Y. Katsuyama, T. Kurokawa and Y. Osada, *Adv. Mater.*, 2003, **15**, 1155–1158.

11 K. Singh, A. Ohlan, P. Saini and S. K. Dhawan, *Polym. Adv. Technol.*, 2008, **19**, 647–657.

12 J. Y. Sun, X. Zhao, W. R. K. Illeperuma, O. Chaudhuri, K. H. Oh, D. J. Mooney, J. J. Vlassak and Z. Suo, *Nature*, 2012, **489**, 133–136.

13 E. Ducrot, Y. Chen, M. Bulters, R. P. Sijbesma and C. Creton, *Science*, 2014, **344**, 186–190.

14 K. Sato, T. Nakajima, T. Hisamatsu, T. Nonoyama, T. Kurokawa and J. P. Gong, *Adv. Mater.*, 2015, **27**, 6990–6998.

15 X. Chen, M. A. Dam, K. Ono, A. Mal, H. Shen, S. R. Nutt, K. Sheran and F. Wudl, *Science*, 2002, **295**, 1698–1702.

16 D. Montarnal, M. Capelot, F. Tournilhac and L. Leibler, *Science*, 2011, **334**, 965–968.

17 K. Imato, M. Nishihara, T. Kanehara, Y. Amamoto, A. Takahara and H. Otsuka, *Angew. Chem., Int. Ed.*, 2012, **51**, 1138–1142.

18 A. Ciferri, *Supramolecular Polymers*, Marcel Dekker Inc., New York, 2000.

19 R. J. Wojtecki, M. A. Meador and S. J. Rowan, *Nat. Mater.*, 2011, **10**, 14–27.

20 N. Holten-Andersen, M. J. Harrington, H. Birkedal, B. P. Lee, P. B. Messersmith, K. Y. C. Lee and J. H. Waite, *Proc. Natl. Acad. Sci. U. S. A.*, 2011, **108**, 2651–2655.

21 Y. Gu, E. A. Alt, H. Wang, X. Li, A. P. Willard and J. A. Johnson, *Nature*, 2018, **560**, 65–69.

22 S. Burattini, H. M. Colquhoun, J. D. Fox, D. Friedmann, B. W. Greenland, P. J. F. Harris, W. Hayes, M. E. MacKay and S. J. Rowan, *Chem. Commun.*, 2009, 6717–6719.

23 S. Burattini, B. W. Greenland, D. H. Merino, W. Weng, J. Seppala, H. M. Colquhoun, W. Hayes, M. E. MacKay, I. W. Hamley and S. J. Rowan, *J. Am. Chem. Soc.*, 2010, **132**, 12051–12058.

24 J. Fox, J. J. Wie, B. W. Greenland, S. Burattini, W. Hayes, H. M. Colquhoun, M. E. MacKay and S. J. Rowan, *J. Am. Chem. Soc.*, 2012, **134**, 5362–5368.

25 K. Haraguchi and T. Takehisa, *Adv. Mater.*, 2002, **14**, 1120–1124.

26 Q. Wang, J. L. Mynar, M. Yoshida, E. Lee, M. Lee, K. Okuro, K. Kinbara and T. Aida, *Nature*, 2010, **463**, 339–343.

27 T. L. Sun, T. Kurokawa, S. Kuroda, A. Bin Ihsan, T. Akasaki, K. Sato, M. A. Haque, T. Nakajima and J. P. Gong, *Nat. Mater.*, 2013, **12**, 932–937.

28 J. C. Lai, L. Li, D. P. Wang, M. H. Zhang, S. R. Mo, X. Wang, K. Y. Zeng, C. H. Li, Q. Jiang, X. Z. You and J. L. Zuo, *Nat. Commun.*, 2018, **9**, 2725.

29 Y. Miwa, K. Taira, J. Kurachi, T. Udagawa and S. Kutsumizu, *Nat. Commun.*, 2019, **10**, 1828.

30 S. Wang and M. W. Urban, *Nat. Rev. Mater.*, 2020, **5**, 562–583.

31 M. W. Urban, D. Davydovich, Y. Yang, T. Demir, Y. Zhang and L. Casabianca, *Science*, 2018, **362**, 220–225.

32 H. Wang, Y. Yang, M. Nishiura, Y. Higaki, A. Takahara and Z. Hou, *J. Am. Chem. Soc.*, 2019, **141**, 3249–3257.

33 D. C. Tuncaboylu, M. Sari, W. Oppermann and O. Okay, *Macromolecules*, 2011, **44**, 4997–5005.

34 E. A. Appel, F. Biedermann, U. Rauwald, S. T. Jones, J. M. Zayed and O. A. Scherman, *J. Am. Chem. Soc.*, 2010, **132**, 14251–14260.

35 M. Nakahata, Y. Takashima, H. Yamaguchi and A. Harada, *Nat. Commun.*, 2011, **2**, 511.

36 M. Zhang, D. Xu, X. Yan, J. Chen, S. Dong, B. Zheng and F. Huang, *Angew. Chem., Int. Ed.*, 2012, **51**, 7011–7015.

37 Y. Takashima, S. Hatanaka, M. Otsubo, M. Nakahata, T. Kakuta, A. Hashidzume, H. Yamaguchi and A. Harada, *Nat. Commun.*, 2012, **3**, 1270–1278.

38 T. Kakuta, Y. Takashima, M. Nakahata, M. Otsubo, H. Yamaguchi and A. Harada, *Adv. Mater.*, 2013, **25**, 2849–2853.

39 K. Miyamae, M. Nakahata, Y. Takashima and A. Harada, *Angew. Chem., Int. Ed.*, 2015, **54**, 8984–8987.

40 V. Kardelis, K. Li, I. Nierengarten, M. Holler, J. F. Nierengarten and A. Adronov, *Macromolecules*, 2017, **50**, 9144–9150.

41 X. Zhao, X. Chen, H. Yuk, S. Lin, X. Liu and G. Parada, *Chem. Rev.*, 2021, **121**, 4309–4372.

42 J. Liu, C. S. Y. Tan, Z. Yu, N. Li, C. Abell and O. A. Scherman, *Adv. Mater.*, 2017, **29**, 1–7.

43 S. Nomimura, M. Osaki, J. Park, R. Ikura, Y. Takashima, H. Yamaguchi and A. Harada, *Macromolecules*, 2019, **52**, 2659–2668.

44 H. Aramoto, M. Osaki, S. Konishi, C. Ueda, Y. Kobayashi, Y. Takashima, A. Harada and H. Yamaguchi, *Chem. Sci.*, 2020, **11**, 4322–4331.

45 J. Park, S. Murayama, M. Osaki, H. Yamaguchi, A. Harada, G. Matsuba and Y. Takashima, *Adv. Mater.*, 2020, **32**, 2002008.

46 B. V. K. J. Schmidt and C. Barner-Kowollik, *Angew. Chem., Int. Ed.*, 2017, **56**, 8350–8369.

47 R. P. Sijbesma, F. H. Beijer, L. Brunsveld, B. J. B. Folmer, J. H. K. K. Hirschberg, R. F. M. Lange, J. K. L. Lowe and E. W. Meijer, *Science*, 1997, **278**, 1601–1604.

48 B. J. B. Folmer, R. P. Sijbesma, R. M. Versteegen, J. A. J. Van Der Rijt and E. W. Meijer, *Adv. Mater.*, 2000, **12**, 874–878.

49 P. Cordier, F. Tournilhac, C. Soulié-Ziakovic and L. Leibler, *Nature*, 2008, **451**, 977–980.

50 Y. Yanagisawa, Y. Nan, K. Okuro and T. Aida, *Science*, 2018, **359**, 72–76.

51 C.-F. Chow, S. Fujii and J.-M. Lehn, *Angew. Chem.*, 2007, **119**, 5095–5098.

52 M. Burnworth, L. Tang, J. R. Kumpfer, A. J. Duncan, F. L. Beyer, G. L. Fiore, S. J. Rowan and C. Weder, *Nature*, 2011, **472**, 334–337.

This journal is © The Royal Society of Chemistry and IChemE 2022

Mol. Syst. Des. Eng., 2022, **7**, 733–745 | **743**

53 Y. Koyama, *Polym. J.*, 2014, **46**, 315–322.

54 Y. Noda, Y. Hayashi and K. Ito, *J. Appl. Polym. Sci.*, 2014, **131**, 1–9.

55 C. J. Bruson and J. F. Stoddart, *The Nature of The Mechanical Bond: From Molecules to Machines*, John Wiley & Sons, Inc., Hoboken, 2016.

56 A. Harada and M. Kamachi, *Macromolecules*, 1990, **23**, 2823–2824.

57 A. Harada, J. Li and M. Kamachi, *Nature*, 1992, **356**, 325–327.

58 A. Harada, J. Li and M. Kamachi, *Nature*, 1994, **370**, 1992–1994.

59 M. Cesario, J. Guilhem, C. Pascard, C. O. Dietrich, A. Edel, J. P. Sauvage and J. P. Kintzinger, *J. Am. Chem. Soc.*, 1986, **108**, 6250–6254.

60 K. Endo, T. Shiroi, N. Murata, G. Kojima and T. Yamanaka, *Macromolecules*, 2004, **37**, 3143–3150.

61 M. C. Jiménez, C. Dietrich-buchecker and J. Sauvage, *Angew. Chem., Int. Ed.*, 2000, **1**, 3284–3287.

62 M. C. Jimenez-Molero, C. Dietrich-Buchecker and J. P. Sauvage, *Chem. – Eur. J.*, 2002, **8**, 1456–1466.

63 L. Fang, M. Hmadeh, J. Wu, M. A. Olson, J. M. Spruell, A. Trabolsi, Y. Yang, M. Elhabiri and J. F. Stoddart, *J. Am. Chem. Soc.*, 2009, **131**, 7126–7134.

64 P. G. Clark, M. W. Day and R. H. Grubbs, *J. Am. Chem. Soc.*, 2009, **131**, 13631–13633.

65 Y. Okumura and K. Ito, *Adv. Mater.*, 2001, **13**, 485–487.

66 T. Karino, M. Shibayama, Y. Okumura and K. Ito, *Phys. B*, 2006, **385–386 I**, 807–809.

67 Y. Shinohara, K. Kayashima, Y. Okumura, C. Zhao, K. Ito and Y. Amemiya, *Macromolecules*, 2006, **39**, 7386–7391.

68 T. Ogoshi, T. Aoki, S. Ueda, Y. Tamura and T. A. Yamagishi, *Chem. Commun.*, 2014, **50**, 6607–6609.

69 X. Li, H. Kang, J. Shen, L. Zhang, T. Nishi, K. Ito, C. Zhao and P. Coates, *Polymer*, 2014, **55**, 4313–4323.

70 H. Murakami, R. Baba, M. Fukushima and N. Nonaka, *Polymer*, 2015, **56**, 368–374.

71 G. Kali, H. Eisenbarth and G. Wenz, *Macromol. Rapid Commun.*, 2016, **37**, 67–72.

72 J. Watanabe, T. Ooya, K. H. Nitta, K. D. Park, Y. H. Kim and N. Yui, *Biomaterials*, 2002, **23**, 4041–4048.

73 T. Ooya, T. Ichi, T. Furubayashi, M. Katoh and N. Yui, *React. Funct. Polym.*, 2007, **67**, 1408–1417.

74 K. Koyanagi, Y. Takashima, H. Yamaguchi and A. Harada, *Macromolecules*, 2017, **50**, 5695–5700.

75 A. Bin Imran, K. Esaki, H. Gotoh, T. Seki, K. Ito, Y. Sakai and Y. Takeoka, *Nat. Commun.*, 2014, **5**, 1–8.

76 H. Gotoh, C. Liu, A. Bin Imran, M. Hara, T. Seki, K. Mayumi, K. Ito and Y. Takeoka, *Sci. Adv.*, 2018, **4**, 7629.

77 J. H. Seo, M. Fushimi, N. Matsui, T. Takagaki, J. Tagami and N. Yui, *ACS Macro Lett.*, 2015, **4**, 1154–1157.

78 S. Choi, T. woo Kwon, A. Coskun and J. W. Choi, *Science*, 2017, **357**, 279–283.

79 D. J. Yoo, A. Elabd, S. Choi, Y. Cho, J. Kim, S. J. Lee, S. H. Choi, T. woo Kwon, K. Char, K. J. Kim, A. Coskun and J. W. Choi, *Adv. Mater.*, 2019, **31**, 1–10.

80 C. Gong and H. W. Gibson, *J. Am. Chem. Soc.*, 1997, **119**, 8585–8589.

81 S. Li, G. H. Weng, W. Lin, Z. Bin Sun, M. Zhou, B. Zhu, Y. Ye and J. Wu, *Polym. Chem.*, 2014, **5**, 3994–4001.

82 M. Nakahata, S. Mori, Y. Takashima, H. Yamaguchi and A. Harada, *Chem*, 2016, **1**, 766–775.

83 Y. Kobayashi, Y. Zheng, Y. Takashima, H. Yamaguchi and A. Harada, *Chem. Lett.*, 2018, **47**, 1387–1390.

84 S. Y. Zheng, C. Liu, L. Jiang, J. Lin, J. Qian, K. Mayumi, Z. L. Wu, K. Ito and Q. Zheng, *Macromolecules*, 2019, **52**, 6748–6755.

85 H. Ke, L. P. Yang, M. Xie, Z. Chen, H. Yao and W. Jiang, *Nat. Chem.*, 2019, **11**, 470–477.

86 Q. Lin and C. Ke, *Chem. Commun.*, 2022, **58**, 250–253.

87 T. Arai, K. Jang, Y. Koyama, S. Asai and T. Takata, *Chem. – Eur. J.*, 2013, **19**, 5917–5923.

88 C. Gong and H. W. Gibson, *J. Am. Chem. Soc.*, 1997, **119**, 5862–5866.

89 K. Iijima, Y. Kohsaka, Y. Koyama, K. Nakazono, S. Uchida, S. Asai and T. Takata, *Polym. J.*, 2014, **46**, 67–72.

90 J. Sawada, D. Aoki, S. Uchida, H. Otsuka and T. Takata, *ACS Macro Lett.*, 2015, **4**, 598–601.

91 J. Sawada, D. Aoki, M. Kuzume, K. Nakazono, H. Otsuka and T. Takata, *Polym. Chem.*, 2017, **8**, 1878–1881.

92 K. Iijima, D. Aoki, H. Otsuka and T. Takata, *Polymer*, 2017, **128**, 392–396.

93 T. Kureha, D. Aoki, S. Hiroshige, K. Iijima, D. Aoki, T. Takata and D. Suzuki, *Angew. Chem., Int. Ed.*, 2017, **56**, 15393–15396.

94 J. Sawada, D. Aoki, H. Otsuka and T. Takata, *Angew. Chem.*, 2019, **131**, 2791–2794.

95 L. Li, Q. Lin, M. Tang, E. H. R. Tsai and C. Ke, *Angew. Chem.*, 2021, **133**, 10274–10281.

96 N. Ogata, K. Sanui and J. Wada, *J. Polym. Sci., Polym. Lett. Ed.*, 1976, **14**, 459–462.

97 Y. Delaviz and H. W. Gibson, *Macromolecules*, 1992, **25**, 4859–4862.

98 T. Murakami, B. V. K. J. Schmidt, H. R. Brown and C. J. Hawker, *J. Polym. Sci., Part A: Polym. Chem.*, 2017, **55**, 1156–1165.

99 S. Ikejiri, Y. Takashima, M. Osaki, H. Yamaguchi and A. Harada, *J. Am. Chem. Soc.*, 2018, **140**, 17308–17315.

100 Y. Takashima, Y. Hayashi, M. Osaki, F. Kaneko, H. Yamaguchi and A. Harada, *Macromolecules*, 2018, **51**, 4688–4693.

101 C. Y. Shi, Q. Zhang, C. Y. Yu, S. J. Rao, S. Yang, H. Tian and D. H. Qu, *Adv. Mater.*, 2020, **32**, 1–7.

102 D. Zhao, Z. Zhang, J. Zhao, K. Liu, Y. Liu, G. Li, X. Zhang, R. Bai, X. Yang and X. Yan, *Angew. Chem.*, 2021, **60**, 16224–16229.

103 H. W. Gibson, D. S. Nagvekar, J. Powell, C. Gong and W. S. Bryant, *Tetrahedron*, 1997, **53**, 15197–15207.

104 H. W. Gibson, D. S. Nagvekar, N. Yamaguchi, S. Bhattacharjee, H. Wang, M. J. Vergue and D. M. Hercules, *Macromolecules*, 2004, **37**, 7514–7529.

105 K. Yamabuki, Y. Isobe, K. Onimura and T. Oishi, *Polym. J.*, 2008, **40**, 205–211.

744 | *Mol. Syst. Des. Eng.*, 2022, **7**, 733–745

This journal is © The Royal Society of Chemistry and IChemE 2022

106 O. Jazkewitsch and H. Ritter, *Macromolecules*, 2011, **44**, 375–382.

107 T. Cai, W. J. Yang, Z. Zhang, X. Zhu, K. G. Neoh and E. T. Kang, *Soft Matter*, 2012, **8**, 5612–5620.

108 T. Murakami, B. V. K. J. Schmidt, H. R. Brown and C. J. Hawker, *Macromolecules*, 2015, **48**, 7774–7781.

109 K. Iwaso, Y. Takashima and A. Harada, *Nat. Chem.*, 2016, **8**, 625–632.

110 A. Goujon, T. Lang, G. Mariani, E. Moulin, G. Fuks, J. Raya, E. Buhler and N. Giuseppone, *J. Am. Chem. Soc.*, 2017, **139**, 14825–14828.

111 R. Ikura, J. Park, M. Osaki, H. Yamaguchi, A. Harada and Y. Takashima, *Macromolecules*, 2019, **52**, 6953–6962.

112 R. Ikura, Y. Ikemoto, M. Osaki, H. Yamaguchi, A. Harada and Y. Takashima, *Polymer*, 2020, **196**, 122465.

113 M. Ogawa, A. Kawasaki, Y. Koyama and T. Takata, *Polym. J.*, 2011, **43**, 909–915.

114 M. B. Yi, T. H. Lee, G. Y. Han, H. Kim, H. J. Kim, Y. Kim, H. S. Ryou and D. U. Jin, *ACS Appl. Polym. Mater.*, 2021, **3**, 2678–2686.

115 Y. Kashiwagi, T. Katashima, Y. Takashima, A. Harada and T. Inoue, *Nihon Reoroji Gakkaishi*, 2019, **47**, 99–104.

116 Y. Kashiwagi, O. Urakawa, S. Zhao, Y. Takashima, A. Harada and T. Inoue, *Macromolecules*, 2021, **54**, 3321–3333.

117 R. A. Fava, *Polymer*, 1968, **9**, 137–151.

118 B. Wuxderlich and D. M. Bodily, *J. Polym. Sci., Polym. Symp.*, 2007, **6**, 137–148.

119 K. Jin, L. Li and J. M. Torkelson, *Polymer*, 2017, **115**, 197–203.

120 R. H. Somani and M. T. Shaw, *Macromolecules*, 1981, **14**, 1549–1554.

121 P. Gardner, R. Lehrle and D. Turner, *J. Anal. Appl. Pyrolysis*, 1993, **25**, 11–24.

122 D. M. Bate and R. S. Lehrle, *Polym. Degrad. Stab.*, 1998, **62**, 57–66.

123 T. Uemura, T. Kaseda, Y. Sasaki, M. Inukai, T. Toriyama, A. Takahara, H. Jinnai and S. Kitagawa, *Nat. Commun.*, 2015, **6**, 1–8.

This journal is © The Royal Society of Chemistry and IChemE 2022

Mol. Syst. Des. Eng., 2022, **7**, 733–745 | **745**